

Ultrahigh-resolution FDOCT system for dermatology

Peter Koch, Dennis Boller, Edmund Koch, Julia Welzel, Gereon Huttmann

Angaben zur Veröffentlichung / Publication details:

Koch, Peter, Dennis Boller, Edmund Koch, Julia Welzel, and Gereon Huttmann. 2005.
"Ultrahigh-resolution FDOCT system for dermatology." In *Coherence domain optical methods and optical coherence tomography in biomedicine IX: 23 - 26 January 2005, San Jose, California, USA*, edited by Valery V. Tuchin, Joseph A. Izatt, and James G. Fujimoto, 24–30. Bellingham, WA: SPIE. <https://doi.org/10.1117/12.592800>.

Nutzungsbedingungen / Terms of use:

licgercopyright

Dieses Dokument wird unter folgenden Bedingungen zur Verfügung gestellt: / This document is made available under these conditions:

Deutsches Urheberrecht

Weitere Informationen finden Sie unter: / For more information see:

<https://www.uni-augsburg.de/de/organisation/bibliothek/publizieren-zitieren-archivieren/publiz/>



Ultra High Resolution FDOCT System for Dermatology

Peter Koch^a, Dennis Boller^a, Edmund Koch^b, Julia Welzel^c, Gereon Hüttmann^a

^{a)} Medizinisches Laserzentrum Lübeck, Peter Monnik Weg 4 23562 Lübeck

^{b)} Technische Universität Dresden, Mendelsohnallee 6, 01309 Dresden

^{c)} Klinik für Dermatologie, University of Luebeck, Ratzeburger Allee 160, 23538 Luebeck

Abstract

We developed an ultra high resolution Fourier-Domain-OCT (FD-OCT) system for the use in dermatology. An axial resolution of less than 3 μm within the tissue was achieved by superimposing two broadband SLDs. FDOCT systems offer new possibilities for the design of the interferometer and the application system. Since no phase modulator is needed, the reference plane can be realized within the application system. This leads to a substantial improvement in the sensitivity against polarisation mode dispersion (PMD). It furthermore makes an elaborate chromatic dispersion matching obsolete. Two different application systems were compared. In the first system the reference wave was created by a plane plate just a few 100 μm above the probe. In the second approach an extra beam splitter and a mirror to generate the reference wave was used.

Introduction

Optical coherence tomography (OCT) was successfully used for imaging upper structures of the skin [1,2]. With a resolution below 15 μm , OCT shows more details of the upper skin morphology than high frequency ultrasound. Additionally OCT works without tissue contact and can therefore be used for quantitative measurement of the thickness of the different skin layers.

Fourier-domain OCT (FD-OCT) has the potential of fast, high-resolution OCT with moderate technical complexity, due to the superior SNR and exchange of the moving delay line by a line detector. The potential of these technique was demonstrated first for high-resolution imaging of the retina. Up to now high resolution imaging of the skin, which is able to resolve the stratum corneum, was only possible with very complex OCT system, which either use a fs-laser or a dynamic focus [3]. Therefore by combining two superluminescent diodes (SLD) we designed and tested an compact FD OCT system with a handheld scan head with a longitudinal resolution of less than 3 μm . This well known approach [4,5] is suitable to generate ultra broadband spectra. Compared with ultra short pulse laser systems the superluminescence diodes used here are cost effective and highly reliable.

Experimental Setup

Fig. 1A shows the optical set up of the spectral radar system. The light of two SLDs (Superlum SLD37MP, $\lambda_c=830$ nm, FWHM=45 nm and Superlum SLD48MP, $\lambda_c=910$ nm, FWHM=90 nm) is combined with a fibre optic beam splitter.

The source light is then directed through a second fibre coupler to the application system. As described below the light is divided into reference- and probe intensity. Both probe and reference light return through the same fibre towards a spectrometer situated in the detection arm of the interferometer. The spectrometer consist of a 20 mm achromatic collimating lens, a 1200 lines/mm reflection grating set close to the Littrow angle, and a 35 mm focal length achromatic imaging lens. The light is focused on a CMOS sensor (Photon Vision Systems LIS 1024, pixel size $8\ \mu\text{m} \times 125\ \mu\text{m}$, 1024 pixel). The spectrum imaged on the sensor covers the range from 810 to 970 nm. The optical system was designed to be diffraction limited to spectral resolution of 0,15 nm. The axial scan range is 1,19 mm in air. Fig. 1B shows a photograph of the assembled system. Data was acquired with a rate of 330 kHz with a standard data acquisition board.

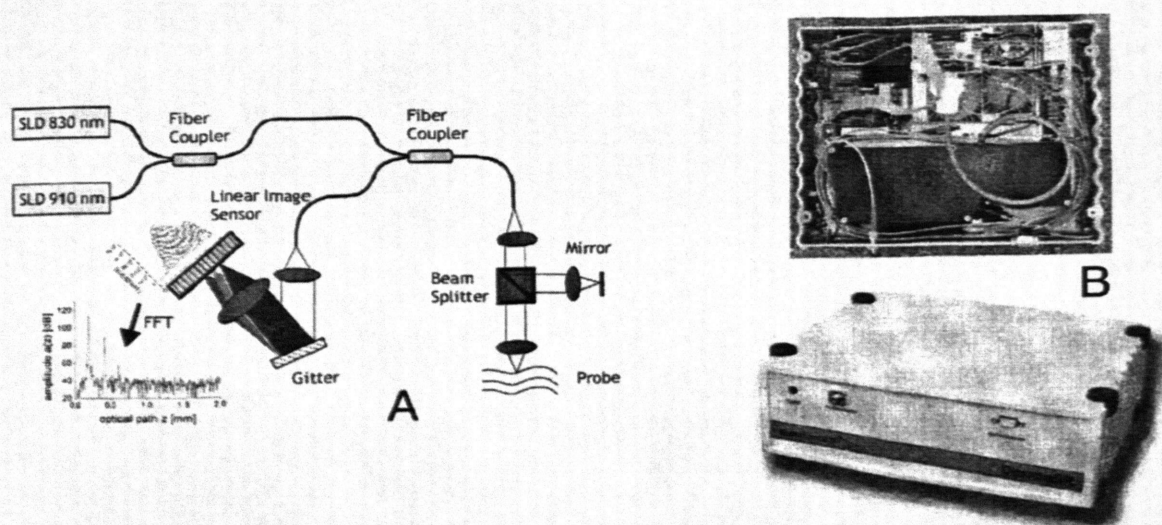


Fig. 1: A)

Experimental set up of the high resolution OCT system. B) Photography of the device used for the clinical study.

Reference measurements were made with a 1300 nm time-domain OCT system with 15 nm resolution described in [1,2] and the SkinDex 300 system from ISIS-Optronics.

The application system

Application systems for OCT have two major purposes: Creating a diffraction limited spot in the tissue and providing possibilities to move that spot transversely over the tissue. It has been shown that a numerical aperture of 0,05 for the focusing optics gives best results for highly scattering tissue. A galvanometric scanner was used to position the spot on the probe. In time domain OCT systems the reference beam usually has been created in the second arm of a fibre optic interferometer by a phase modulator. Due to the fact that FDOCT systems don't need a phase modulator they offer the option to create the reference wave within the application system. Fig. 2 shows two different approaches.

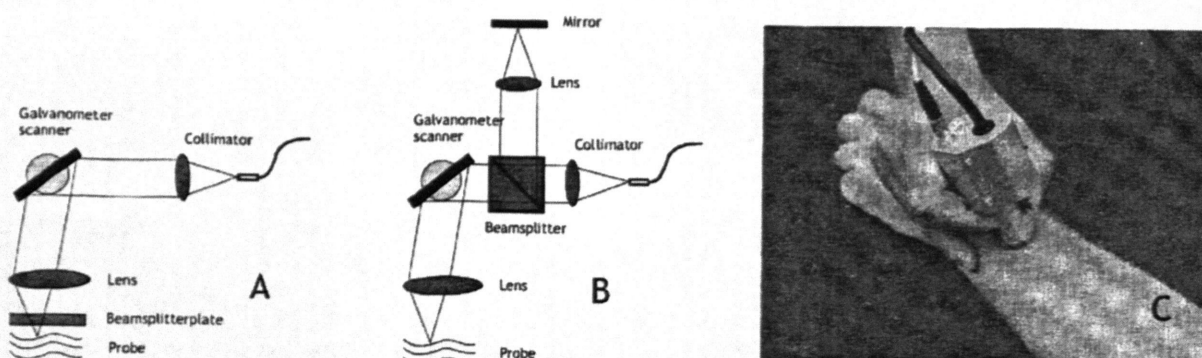


Fig. 2: Two approaches to an application systems with integrated reference arm. (A) shows a system with were the reference wave is created by a beam splitter plate placed a few 100 μm above the tissue under investigation. (B) shows a approach with a beam splitter cube and a reference mirror.

Both set-ups have the advantage, that probe- and reference light share the same fibres on their way to the detection unit. Therefore all fibre induced distortions are cancelled out. Both principles have been implemented in an application system depicted in Fig. 2C and tested in the clinic for dermatology.

In the 'type A' application system [6] a beam splitter plate with a thickness of 5 mm was used to generate the reference wave. On the surface directed towards the probe a coating with a reflectivity of 20% was applied. The top surface had an antireflection coating. Both the thickness of the plate of 5mm and the AR coating were chosen to prevent a secondary reference wave from the second surface of the plate. The set up has the advantage that the loss to the probe light is only 36% (0,8x0,8) and that the optical layout is very simple. Due to the fixed distance between the reference mirror and the probe, no adjustments of the reference arm length is required. The application system was designed, so that the reflecting side of the plate was approximately 200 μm above the tissue.

For best image quality the focus plane of an OCT application system has to be placed a few 100 μm beyond the surface. In our set up that also means that the reference plane is at least few hundred μm out of focus. Fig. 3 displays the experimentally measured loss of reference intensity due to defocusing for different numerical apertures.

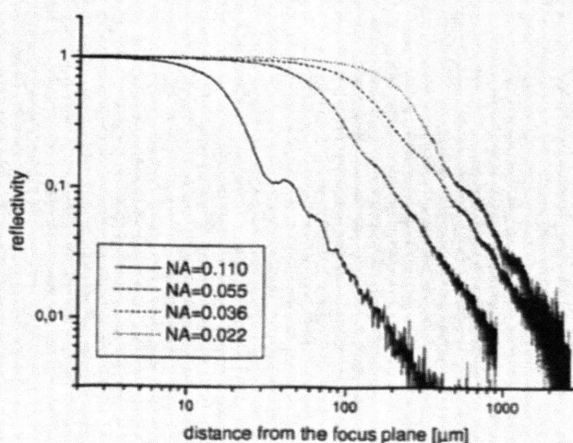


Fig. 3 Fraction of light reflected from the surface of the beam splitter plate back into the fibre versus the distance between the focus plane and the surface of the mirror. For higher numerical apertures the reference intensity drops faster with defocussing.

For the desired numerical aperture of 0,05 the intensity of the reference wave is already attenuated by one orders of magnitude for a defocusing of only 200 μm . To get a reasonable reference intensity coupled back into the fibre the focus plane has either to be moved towards the reference mirror or the numerical aperture has to be reduced. For the clinical system we have chosen a numerical aperture of 0,022. This was not optimal, but it is a reasonable compromise between resolution and reference intensity. During the clinical evaluation we observed additional problems with this approach. The reference surface was distorted by dust and condensing water. This influenced the reference intensity in a site depended fashion. In the application system depicted in Fig 2 B a separate reference wave is created by a beam splitter cube. This has the advantage, that the reference intensity is independent of the position of the focus plane on the probe. In this design it can actually be adjusted by defocusing the reference mirror. But this set up also requires an adjustment of the reference arm length. This was implemented by moving the lens and mirror assembly together along the beam path. Here the numerical aperture of the probe optics can be chosen without any restrictions. For the clinical device a NA of 0,042 was used. Of cause the use of a beam splitter cube, that has to be passed two times by the reference light, causes a higher loss of probe intensity if compared with the direct reflection in the above design.

Spectral shaping

Image sensors used for FDOCT systems have a relatively high deviation between the sensitivity of different pixels. For the sensor used the pixel response non uniformity (PRNU) is specified with 0,5%. To gain a shot noise limited dynamic range this systematic measurement error has to be removed. The straightest approach would be the determination of the PRNU before mounting the sensor in the spectrometer by illuminating it evenly and recording the response of each pixel. We use a different approach that enables us to repeat the calibration process as often as necessary and additionally allows us to shape the spectrum of the light source to a chosen normalization function at the same time. To shut down probe light temporarily the galvanometer scanner mirror from Fig. 2B is driven to maximal displacement. Under these conditions the spectrum of the light source $PR(n)$ is measured by the spectrometer. By dividing $PR(n)$ by a chosen normalization function $NS(n)$ a correction vector is calculated that can be used to remove all imperfections introduced by the light source and the image sensor. This approach has the advantage, that no additional information about the image sensor or the light source is needed. For our experiments we usually use a Hanning window as the normalization function, because this function has a very narrow fourier transform without significant side lobes.

The influence of the shape of the coherence function on the quality of OCT images was determined. For this purpose we designed the three normalization spectra displayed in Fig. 4. The first resembles the spectral density function of the two combined SLD sources used in the setup. We modelled this spectrum by combining four Gaussian functions. The second is our standard Hanning window function. The third Function resembles a spectral density typical for fs laser systems.

The corresponding coherence functions are displayed in Fig. 4 on a log scale. From this it can be seen that the coherence length stated as the FWHM is similar for all spectra. It can also be seen, that the coherence function resulting from the two SLD spectrum has significant side lobes (first -15 dB @ 15 μm) whereas the coherence functions resulting from Hanning window shaped spectral densities drop to -50 dB without any side lobes.

The images in Fig. 5 show measurements of an onion processed with the three different normalization spectra. In comparison the images where the Hanning window was used shows a significantly better resolution than the images based on the spectral density function of two combined SLDs.

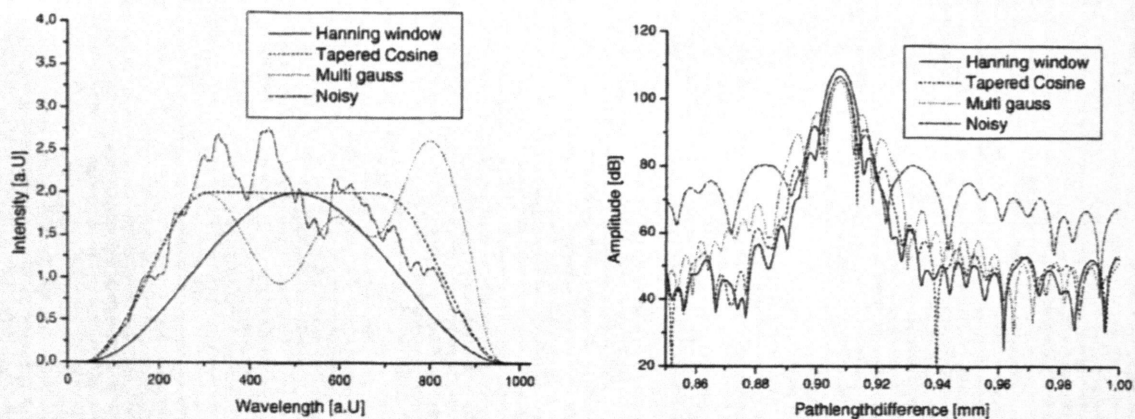


Fig. 4: Spectral density functions and corresponding coherence functions of the windows used to deconvolute the OCT images shown in Fig. 5.

Methods to reshape the spectral density function of OCT light sources are known from the literature as spectral shaping. It can either be done by introducing a matched optical filter into the interferometer [7,8]. Others have suggested a scheme where the time domain OCT signal gets fourier transformed into frequency space processed there and finally gets back transformed into time space [9-11]. The first method requires elaborate additional optics, the second approach has to cope with the phase instability of TD OCT systems. In contrast the method demonstrated here only requires a simple scaling operation.

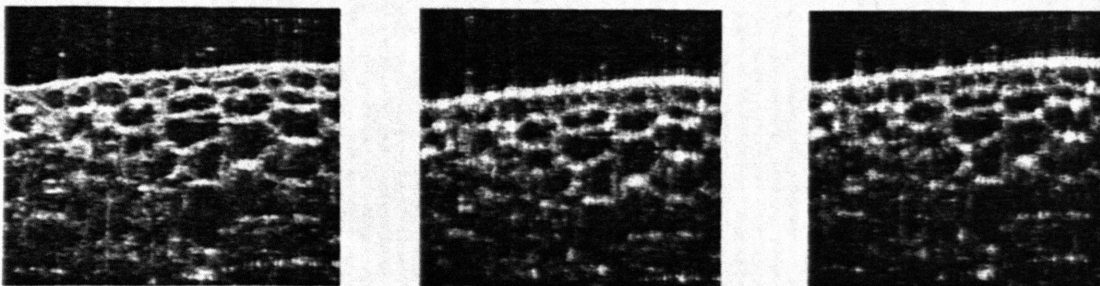


Fig. 5: B-scan image of of onion cells. The image dimensions are $940\mu\text{m} \times 2\text{mm}$ at a lateral resolution of $10\mu\text{m}$.

Clinical Measurements

Fig. 6 depicts an OCT image of skin at the fingertip with an 1300nm time domain OCT system, measured with a axial resolution of $16\mu\text{m}$. The image inserted in the upper right corner was generated with the high resolution OCT system described here. In both images the stratum corneum layer and the epidermis can be distinguished easily. The high resolution image shows a smaller speckle grain size, and therefore appears smoother. The vertical zigzag structures within the stratum corneum are sweat glands. In the high resolution image these structures show in more details.

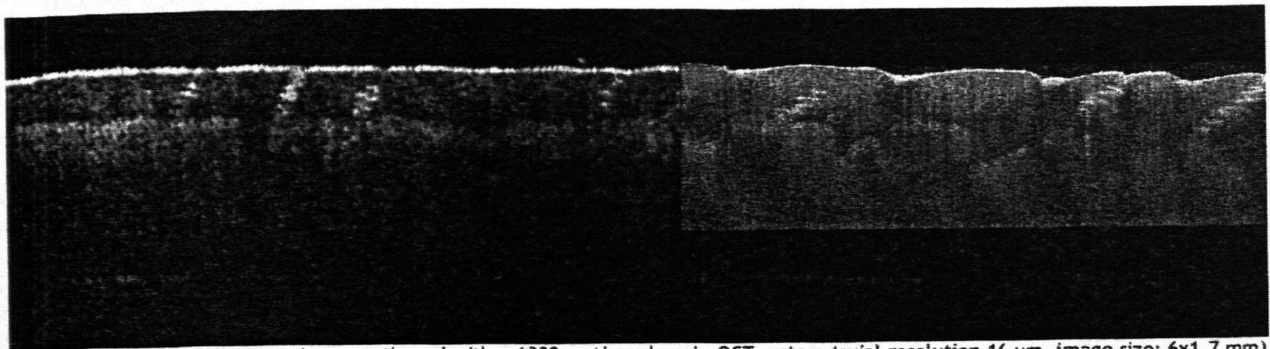


Fig. 6: Comparison between an image gathered with a 1300nm time domain OCT system (axial resolution 16 μm , image size: 6x1,7 mm) and an image gathered with the described high resolution Fourier domain OCT system (axial resolution of 4 μm , image size 2x0,9 mm).

The FD-OCT system was compared with the commercially available dermatological OCT device SkinDex 300 from ISIS Optronics. The resolution is specified with 5 μm axial and 3 μm lateral over the entire depth scanning range. The high lateral resolution is achieved by adjusting the focus position during the a-scan. To compensate the speed penalty introduced by the slow focusing optics 8 A-scans are sampled simultaneously at different lateral positions.

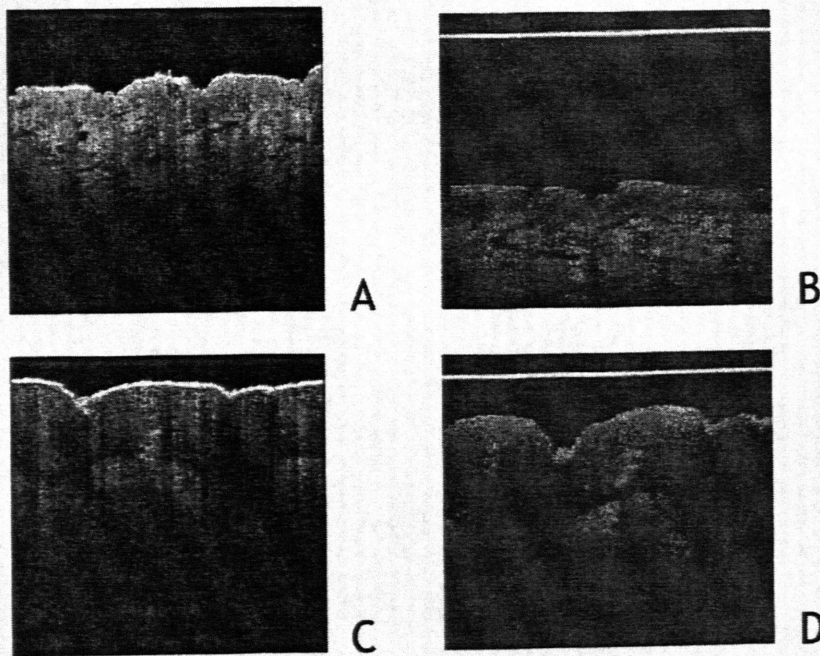


Fig.: 7: Comparison between measurements made with a SkinDex 300 (right column B and D) and the device described here (left column A and C). The upper row (A, B) shows measurements performed at the lower arm. Images on the lower row (C, D) were measured at the thumb.

The Fig. 7A and 7C show FD-OCT images of the lower arm and the thumb. At the same locations images were taken with the SkinDex 300 (Fig. 7B and 7D). The bright stripe at the upper image boundary originates from the exit window of the application system of the device. A comparison of the images doesn't show a significant difference in image quality although the SkinDex is the far more complex system. Fig. 8 demonstrates that the FD-OCT system is able to resolve the stratum corneum at the inner side of the hands, which is only 5-10 μm thick.

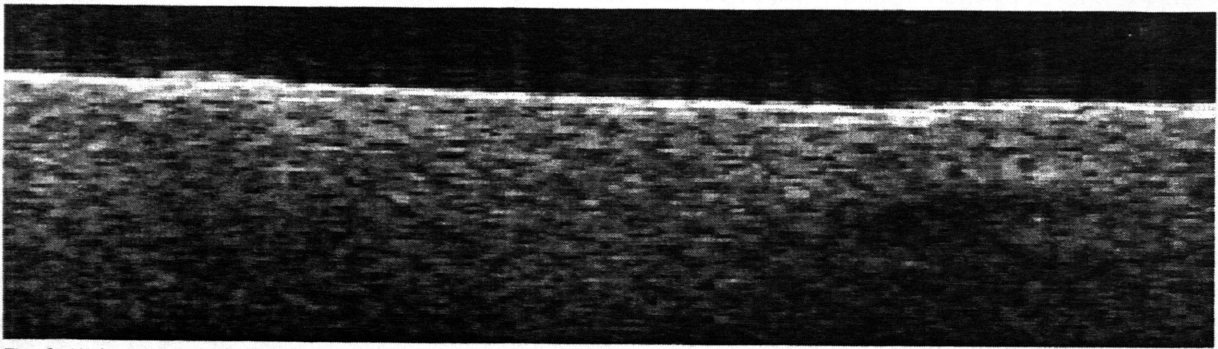


Fig. 8: High resolution OCT image of the inner side of the under arm. Image size: 08x0,3 mm

Conclusion

We have designed a FD-OCT system with an axial resolution of less than $4\text{ }\mu\text{m}$ by combining 2 SLD light sources. We described an easy to implement method to remove the side lobes of the coherence function, that arise from the non ideal shape of the spectrum. Our novel application system design compensates dispersion and length matching problems.

Finally superior image quality was demonstrated by comparing measurements performed with a previously used time domain OCT system and a commercially available OCT system with the developed device. Advantage of the FD-OCT system is the compact, hand-held scanhead.

References

1. J. Welzel, E. Lankenau, R. Birngruber, R. Engelhardt (1997). "Optical coherence tomography of the human skin." *J Am Acad Dermatol.* 37(6):958-63.
2. J. Welzel (2001) "Optical coherence tomography in dermatology: a review."
3. *Skin Res Technol.* 7(1):1-9.
4. A. Knüttel, S. BonevS, W. Knaak (2004) "New method for evaluation of in vivo scattering and refractive index properties obtained with optical coherence tomography." *J Biomed Opt.* 9(2):265-73.
5. Y. Zhang, M. S., N. Tanno (2001). "Resolution improvement in optical coherence tomography by optimal synthesis of light-emitting diodes." *Optics Letters* 26(4): 205-208.
6. Y.J. Rao, Y. N. N., D.A. Jackson (1993). "Synthesized source for white-light sensing systems." *Optics Letters* 18(6): 462-465.
7. A. Vakhtin, D. J. K., W.R. Wood, K.A. Peterson (2003). "Common-path interferometer for frequency-domain optical coherence tomography." *Applied Optics* 42(34): 6953-6958.
8. Q. Wang, Y. Z., Y. Soh (2004). "Design of spectrum equilization filter for SLED light source." *Optics Communications* 229(229): 223-231.
9. A.C. Akcay, J. P. R., J.M. Eichenholz (2003). "Spectral shaping to improve the point spread function in optical coherence tomography." *Optics Letters* 28(20): 1921-1924.
10. J.F. deBoer, C. E. S., J.S. Nelson (2001). "Stable Carrier generation and phase-resolved digital data procesing in optical coherence tomography." *Applied Optics* 40(31): 5787-5790.
11. M. Bachkansky, M. D. D., J. Reintjes and P.R. Battle (1998). "Signal Processing for Improving Field Cross-correlation Function in Optical Coherence Tomography." *Applied Optics* 37: 8137-8138.
12. R. Tripathi, N. N., J.S. Nelson, B.H. Park and J.F. deBoer (2002). "Spectral shaping for non-Gaussian source spectra in optical coherence tomography." *Optics Letters* 27(6): 406-409.